Arteriosclerosis, Thrombosis, and Vascular Biology

Check for updates

BASIC SCIENCES

Single-Cell RNA Sequencing Reveals That Adaptation of Human Aortic Endothelial Cells to Antiproliferative Therapies Is Modulated by Flow-Induced Shear Stress

Antonio G. Salazar-Martín,* Aditya S. Kalluri,* Martin A. Villanueva, Travis K. Hughes, Marc H. Wadsworth II, Tyler T. Dao, Mercedes Balcells, Farhad R. Nezami, Alex K. Shalek, Elazer R. Edelman

BACKGROUND: Endothelial cells (ECs) are capable of quickly responding in a coordinated manner to a wide array of stresses to maintain vascular homeostasis. Loss of EC cellular adaptation may be a potential marker for cardiovascular disease and a predictor of poor response to endovascular pharmacological interventions such as drug-eluting stents. Here, we report single-cell transcriptional profiling of ECs exposed to multiple stimulus classes to evaluate EC adaptation.

METHODS: Human aortic ECs were costimulated with both pathophysiological flows mimicking shear stress levels found in the human aorta (laminar and turbulent, ranging from 2.5 to 30 dynes/cm^2) and clinically relevant antiproliferative drugs, namely paclitaxel and rapamycin. EC state in response to these stimuli was defined using single-cell RNA sequencing.

RESULTS: We identified differentially expressed genes and inferred the TF (transcription factor) landscape modulated by flow shear stress using single-cell RNA sequencing. These flow-sensitive markers differentiated previously identified spatially distinct subpopulations of ECs in the murine aorta. Moreover, distinct transcriptional modules defined flow- and drug-responsive EC adaptation singly and in combination. Flow shear stress was the dominant driver of EC state, altering their response to pharmacological therapies.

CONCLUSIONS: We showed that flow shear stress modulates the cellular capacity of ECs to respond to paclitaxel and rapamycin administration, suggesting that while responding to different flow patterns, ECs experience an impairment in their transcriptional adaptation to other stimuli.

GRAPHIC ABSTRACT: A graphic abstract is available for this article.

Key Words: cardiovascular diseases ■ endothelial cells ■ humans ■ paclitaxel ■ sirolimus ■ transcription factors

Downloaded from http://ahajournals.org by on July 13, 2026

Maintaining vascular homeostasis is fundamental to the regulation of blood flow, hemostasis, solute transport, and immunologic response. Endothelial cells (ECs) are the cornerstone of vascular regulation, comprising the endothelium, the inner layer of blood vessels in contact with the bloodstream. ECs are the main regulators of vascular homeostasis, by (1) sensing flow fluctuations and modifying vascular tone, (2) regulating hemostasis, (3) acting as permeability gatekeepers, and (4) enabling the immune response.[1]

See accompanying editorial on page 2282

ECs are capable of quickly responding in a coordinated manner to the entire array of stresses present in the vasculature. Biochemical (vascular signaling mediators such as TNF-α [tumor necrosis factor alpha], IL [interleukin]-1β, or Ox-LDL [oxidized low-density lipoprotein]), biomechanical (hemodynamic forces or mechanical stretches such as shear stress, hemodynamic

Correspondence to: Elazer R. Edelman, Massachusetts Institute of Technology, 400 Main St, Bldg E25-438, Cambridge, MA 02142. Email ere@mit.edu
*A.G. Salazar-Martín and A.S. Kalluri contributed equally.
Supplemental Material is available at https://www.ahajournals.org/doi/suppl/10.1161/ATVBAHA.123.319283.
For Sources of Funding and Disclosures, see page 2279–2280.
© 2023 The Authors. *Arteriosclerosis, Thrombosis, and Vascular Biology* is published on behalf of the American Heart Association, Inc., by Wolters Kluwer Health, Inc. This is an open access article under the terms of the Creative Commons Attribution Non-Commercial-NoDerivs License, which permits use, distribution, and reproduction in any medium, provided that the original work is properly cited, the use is noncommercial, and no modifications or adaptations are made.
Arterioscler Thromb Vasc Biol is available at www.ahajournals.org/journal/atvb

Nonstandard Abbreviations and Acronyms

DEG	differentially expressed gene
EC	endothelial cell
GSEA	gene set enrichment analysis
HAEC	human aortic endothelial cell
IL	interleukin
mTOR	mammalian target of rapamycin
PC	principal component
RGS5	regulation of G protein signaling 5
scRNA-seq	single-cell RNA sequencing
TF	transcription factor
TNF-α	tumor necrosis factor alpha
WGCNA	whole-genome correlation network analysis

Highlights

- Flow shear stress commits endothelial cells to identifiable cellular states.
- The identification of differentially expressed genes and transcription factors sensitive to flow-induced shear stress helps in characterizing endothelial cell subpopulations in the aorta.
- Well-localized endothelial cell subpopulations in the aorta express varying flow sensitivities.
- The concomitant exposure of endothelial cells to flow drives them to specific states that restrict their ability to respond to antiproliferative therapies.
- Altered flow reduces the response and the functional modules involved in endothelial cell response to paclitaxel and rapamycin administration.

pressure, or vasodilatation/vasoconstriction), and cell-derived environmental stimuli or alterations induced during endovascular treatments (eg, endothelial rupture, drug stimulation) are sensed by ECs and drive ECs to commit to specific reactive programs.[2] Because ECs perform so many complementary functions, each potential stimulus may lead to a wide array of overlapping fluctuations in the transcriptome and secretome.[3]

EC dysfunction in response to pathology disturbs the nonmigrating, nonproliferating quiescent state; thus, EC state can be used as a mirror of vascular integrity and overall health. Studying EC states in different pathophysiological contexts is crucial to (1) add to our understanding of how and why vascular response to pharmaceuticals differs across target lesions, organs, and people and (2) define novel markers of vascular disease, the leading cause of death globally.[4] Here, we hypothesize that loss of EC cellular adaptation may be an early indicator of vascular disease and a predictor of poor response to clinical intervention.

Addressing this hypothesis first requires identifying paradigmatic stimuli from distinct classes that are known to induce state changes in ECs. We chose 2 orthogonal classes of stress: mechanically mediated (flow-induced shear stress) and chemically medicated (antiproliferative drugs released from indwelling endovascular implants such as drug-eluting stents). Shear stress is a well-known mechanical stimulus driving EC state.[5–7] Variations in shear stress levels induce broad phenotypic switching in ECs.[2,6] Alterations in shear exposure are implicated in almost every biological function of ECs, including gene expression,[8] endoplasmic reticulum stress,[9] mitochondrial function,[10] and epigenetic regulation.[11] Additionally, ECs are the first cells exposed to pharmacological agents, and as such, antiproliferative drugs like rapamycin and paclitaxel are also known drivers of the EC state. Rapamycin and its analogs are compounds with complex biology,[12] most recently assuming prominence in vascular biology by virtue of their use in drug-eluting stents. Here, locally delivered rapamycin influences EC proliferation and migration with uncertain cytotoxicity.[13] Rapamycin and related analogs impact the EC state via action on mTOR (mammalian target of rapamycin) and by altering EC calcium dynamics.[14] Paclitaxel—a member of the taxane class of drugs—is a compound used to avoid restenosis because it is a potent inhibitor of EC proliferation and angiogenesis by modulating the activity of α/β-tubulin heterodimers (microtubules) that conforms the dynamic cell cytoskeleton.[15]

Shear stress and rapamycin/paclitaxel are not necessarily truly independent stimuli. For example, rapamycin also influences ECs by direct activation of vasoactive receptor families[16] including eNOS and by impact on key endothelial TFs (transcription factors) including KLF2[17]; the eNOS and KLF2 pathways are themselves shear responsive. Activation of mTOR has also been implicated in the atheroprone effect of altered shear stress via its effect on autophagy.[18] Thus, shear stress and rapamycin/paclitaxel represent distinct stimuli with broad effects on disease-relevant EC states. Understanding these effects in combination at single-cell resolution will elucidate how complex microenvironments may modulate EC dynamism.

Previously, single-cell transcriptomics has been used to describe EC state in the context of biological processes such as angiogenesis[19,20] and environmentally driven processes such as diet alteration[21,22] and disturbed flow.[23] Some authors have also explored the role of shear stress in EC with single-cell RNA sequencing (scRNA-seq). In this study, we used Seq-Well[24]—a picowell-based scRNA-seq platform—to build upon previously explored markers of shear stress in ECs[25] and define the components of EC cellular adaptation to a combination of pathophysiological shear stresses and chemical stimuli under controlled conditions. This allows us to understand how EC cellular adaptation differs when ECs

Downloaded from http://ahajournals.org by on July 13, 2026

are committed to different flows in a highly controlled, stimulus-specific analysis.

Using our scRNA-seq profile of aortic ECs under well-controlled pathophysiological flows, we detected differentially expressed genes (DEGs) and defined the TF landscape influenced by flow-induced shear stress. These markers were sufficient to differentiate previously defined distinct subpopulations of ECs in scRNA-seq data from murine aorta, exhibiting varying flow sensitivities in spatially distinct domains.

Next, we investigated the influence of dual-stimulus classes on ECs and defined the modular components of the EC response to rapamycin and paclitaxel under varying flow-induced shear stress. We demonstrated that the application of mechanical stimulation via shear stress alters the EC response to antiproliferative agents. This suggests that ECs change responsiveness to stimulation once committed to a stimulus such as different levels of flow-induced shear stress and may serve to explain the diverse drug responses in ECs observed across different target lesions, organs, and people in a clinical setting.

Downloaded from http://ahajournals.org by on July 13, 2026

METHODS

Data Availability

Data presented in this study are available at Gene Expression Omnibus, reference number GSE212388 (token: ovapmmqmntcbpwz). All software required to reproduce figures is open source. Code to reproduce presented figures is available on Github. Please see the Major Resources Table in the Supplemental Material for further information.

EC Culture

A combination of primary human aortic ECs (HAECs; PromoCell) isolated from both the ascending and descending aortas at passage P5 was used for all experiments. The media used for cell culture (Lonza EGM-2 or PromoCell Growth Medium 2) and in the flow-controlled bioreactor was supplemented to a total serum concentration of 7% using fetal bovine serum. Media was additionally supplemented with 100 U penicillin/mL, 100 µg streptomycin/mL, and 1 µg amphotericin/mL.

Multimodal Culture of ECs in a Flow-Controlled Bioreactor

A previously described controllable flow loop bioreactor system was utilized for culture of HAECs under laminar high/physiological and low/altered-flow shear stress conditions.[26] Briefly, the flow loop was driven by a peristaltic pump (ISMATEC MCP, product No. 78002-00) with an attached 8-roller, 12-channel pump head (ISMATEC Type IBM733A, product No. 78002-36). ISMATEC PharMed BPT pump tubing with an internal diameter of 2.79 mm (Cole Parmer) was utilized in the flow loop. Silastic laboratory tubing with an internal diameter of 0.188 in/4.78 mm and an outer diameter of 0.312 in/7.92 mm (Dow Corning) connected the pump tubing and the cell culture chamber to a custom glass media reservoir, and 3/16″×3/32″ tubing connectors (Cole Parmer) connected the pump tubing and the Silastic tubing. The non–cell chamber components of the flow loop were preassembled and autoclaved before flow loop assembly.

For the laminar high- and low-flow shear stress experiments, HAECs were seeded in Ibidi µ-Slide I Luer 0.8 flow chambers with ibiTreat proprietary tissue culture coating for all experiments. These chambers have a height of 800 µm, a channel volume of 200 µL, a channel length of 50 mm, a channel width of 5 mm, a reservoir volume of 60 µL, and a growth area of 2.5 cm^2 per channel. Ibidis were seeded with 200 µL of HAECs at a 0.6 to 1.2 million cells/mL concentration at least 12 hours before connecting to flow; cell attachment and confluence were confirmed by microscopy before initiating shear conditioning. Pump flow rates were set to achieve shear stresses of 30 and 2.5 dynes/cm^2 for high and low shear experiments, respectively.

In this study, turbulent flow and numerically quantified wall shear stress on HAECs was also simulated. HAECs were seeded in a custom-made chamber with a narrow channel (1-mm wide, 2-mm high, and 5-mm long), which transitioned into a wider section (3.6-mm wide, 2-mm high, and 15-mm long). An oscillatory volumetric flow with an amplitude of 160 mL/min and a frequency of 1 Hz was applied at the inlet, leading to shear stresses ranging from 0 to 65 dynes/cm^2. The simulation of the chamber was conducted using Fluent 2022 R2 (ANSYS, Inc, Canonsburg, PA), utilizing the viscous k-omega model due to its superior performance in resolving internal and separated flows, as well as local recirculation. Chamber's walls were modeled as stationary, no-slip boundaries. To account for the entrance region (21.7 mm), both tubes at the inlet and outlet were included in the experiment. The computational domain was meshed using ≈4.5 million polyhedral cells after mesh independence for the solution was confirmed. The cell media was modeled as a Newtonian fluid with a density of 997 kg/m^3 and a viscosity of 6.91×10^{-4} $kg{\cdot}m^{-1}{\cdot}s^{-1}$. At the maximum volumetric flow rate (160 mL/min), the Reynolds number was calculated to be 2564 in the narrower channel, justifying our decision to model the flow as turbulent.

To fabricate the chamber, a mold made of stacked layers of polymethyl methacrylate was laser-cut using an Epilog Laser Fusion 120 W, and polydimethylsiloxane (Sylgard) was poured at a concentration of 1:10 and cured overnight at 70 °C. Plasma bonding between a glass coverslip and the polydimethylsiloxane chamber was achieved using a plasma cleaner (Harrick Plasma; PDC-001) with a pressure controller (Harrick Plasma; PDC-FMG). Two holes were punched into both the inlet and outlet, and tubes were connected and sealed with polydimethylsiloxane before being left overnight at 70 °C. Chambers were autoclaved using a 20/20 cycle and then coated with 1.5 µg/cm^2 of fibronectin solution in PBS for an hour. After 3× 10-minute washes in PBS, HAECs were seeded, and the experiment proceeded similarly to the laminar flow experiments.

Fifteen milliliters of media were used in each flow reservoir to ensure a physiological pH for the total duration of the experiments (72 hours). The oxygenation of medium was accomplished by using oxygen-permeable flow loop tubing.

Unimodal Flow Stimulus Experiment

HAECs were cultured using the flow loop bioreactor system under constant high flow–induced (30 dynes/cm^2), low

flow–induced (2.5 dynes/cm^2), or turbulent flow–induced shear for 72 hours. Following shear culturing, cells were isolated from flow chambers and used as input to Seq-Well for scRNA-seq.

Bimodal Flow and Chemical Stimulus Experiment

HAECs were cultured using the flow loop bioreactor system under constant high (30 dynes/cm^2), low (2.5 dynes/cm^2) or turbulent shear stress for a total of 3 days. Twenty-four hours after the initiation of flow, once ECs have been committed to high, low, or turbulent flow, rapamycin (InSolution, Calbiochem/Sigma-Aldrich) or paclitaxel (Invitrogen, ThermoFisher) dissolved in media was added to two-thirds of the flow loops to achieve a final concentration of 1 and 10 μM, respectively. These concentrations have been previously demonstrated to result in alterations in RNA expression in ECs.[17,27] An equal volume of normal media was added to the nondrug flow loops. Following shear culturing (24 hours without drugs, 48 hours with drugs: a total of 72 hours), cells were isolated from Ibidis and used as input to Seq-Well for scRNA-seq.

Single-Cell Transcriptional Profiling of Cultured ECs via Seq-Well

Following flow conditioning, cells were harvested from Ibidi flow chambers, and scRNA-seq was performed via Seq-Well, an scRNA-seq method developed to be appropriate for low-input (≈10^4 cells) samples.[28] Seq-Well S324 using second-strand synthesis was utilized for all samples. Per condition, 10 000 cells were loaded as the input to Seq-Well.

After amplification, sample libraries were prepared for sequencing using the Nextera XT DNA tagmentation/amplification. Libraries were purified with SPRI (solid-phase reversible immobilization) ratios of 0.6× and 0.8× applied to the amplified and tagmented product, respectively. Final libraries had an average fragment size distribution between 400 and 600 bp. Libraries were loaded onto NextSeq 500 at a final loading concentration of 2.2 pM with a read structure as follows: 20 cycles covering the 12-bp cell barcode and 8-bp unique molecular identifiers (read 1); 50 cycles on the mRNA strand (read 2); 8 cycles covering sample-specific barcode sequences (index 1). Each sample was allotted 200 million reads for a target sequencing depth of 10 000 to 15 000 reads per cell.

Illumina's bcl2fastq software (2.20.0.422) was used to demultiplex samples according to sample-specific indices introduced in the post-tagmentation polymerase chain reaction. The Drop-seq Pipeline maintained by the Broad Institute was used to align raw FASTQ files to the human reference genome and to generate gene count matrices using the default parameters. Mapped reads filtered for quality were used to generate digital gene expression matrices for each sample. Unique molecular identifier–collapsed data were used to generate the final counts table used for analysis; digital gene expression matrices were combined from separate array samples by retaining the genes detected in all samples to generate count tables for further analysis.

Computational Analysis and Cell Quality Control

Raw count tables were used as the input for analysis in the Seurat package for R (version 4.1.0).[29,30] Cells with at least 500 genes and 10 000 molecules detected were retained for analysis; cells with >5\% mitochondrial reads were excluded from analysis. Following quality control, 18 466 cells were analyzed from the in vitro experiments with an average of ≈9194 reads per cell and ≈3017 genes per cell. Normalized expression values were computed for expression in each cell by scaling each cell to 10 000 total unique molecular identifiers and log-normalizing these values with an added pseudocount of 1 using the Seurat NormalizedData function.[29,30] Variable genes were identified using the Seurat FindVariableFeatures function with the VST (variance stabilizing transformation) selection method and 2000 as the number of genes to select as top variable features.[29,30]

High-depth normal mouse aorta transcriptional profiles were downloaded from the Broad Institute Single Cell Portal. ECs were defined based on the expression of the canonical marker Cdh5. A total of 825 ECs were included in the analysis, with an average of 2077 reads per cell and 5900 genes per cell. Data normalization, feature selection, and scaling were performed as previously described above.

Dimensional Reduction of Flow-Conditioned and Dual-Stimulus EC Data

Dimensional reduction of the shear-conditioned EC scRNA-seq profiles was performed on scaled normalized count data using 30 principal components (PCs) based on examination of the PC significance plot. The Seurat implementation of the uniform manifold approximation and projection for dimensional reduction algorithm was used to project 30 PCs into a 2-dimensional space for demonstration of flow state separation.[29,30] Dimensional reduction of dual-stimulus data was accomplished similarly also using 30 PCs.

Differential Expression Analysis

Identification of differentially expressed transcripts between conditions (eg, high/physiological versus low/altered shear states or control versus rapamycin/paclitaxel) was performed using the FindMarkers function in Seurat with a minimum log-fold change threshold of 0.25 and with *P* values computed using a Wilcoxon rank-sum test. Subpopulation-specific markers following cluster analysis were identified using the FindAllMarkers function in Seurat with a minimum log-fold change threshold of 0.25 and with *P* values computed using a Wilcoxon rank-sum test. Gene set enrichment results were robust to ≈5% variations in choice of log-fold change threshold. *P* values were adjusted for multiple hypothesis correction in both cases using a Bonferroni correction based on the total number of genes in the analyzed data set; adjusted $P<0.05$ defined a significant marker. For gene set enrichment analysis (GSEA) plots, differential expression analysis was conducted using R library DESeq2 from Bioconductor (1.32.0).[31] To validate the results and contrast several cluster algorithms to evaluate functional heterogeneity in HAECs, we also computed the results with the scGEAToolbox in MATLAB.[32]

Gene Set Enrichment for Defined Marker Lists

Gene set enrichment on gene lists describing differentially expressed transcripts between 2 conditions or whole-genome correlation network analysis (WGCNA)–derived modules was

Downloaded from http://ahajournals.org by on July 13, 2026

performed using the R library BiocManager (1.18.0)[33] with a *P* value cutoff of 0.05. Annotated gene sets were drawn from a custom GMT (gene matrix transposed) file derived from the canonical pathways and gene ontology gene sets in v6.2 of the Molecular Signatures Database.[34] These include gene sets from the Biocarta, Kyoto Encyclopedia of Genes and Genomes, Reactome, and Gene Ontology databases.

TF Activity Inference

The known targets of each TF in humans were identified using DoRothEA (1.4.2).[35] mRNA expression levels were used to compute TF activity, and only TFs with confidence levels A to C were used for this analysis. DoRothEA regulons were coupled with the statistical method VIPER (1.26.0).[36] The resulting TF activity matrix was then analyzed similarly to gene analysis as explained above.

WGCNA-Inspired Unsupervised Gene Module Identification

DEGs between rapamycin or paclitaxel and control conditions were identified in both high and low shear contexts as described above using a corrected significance threshold but no fold change threshold. Gene modules within these drug response gene sets that were coexpressed were identified using functions from the R WGCNA library.[37] WGCNA was applied with a soft power of 6 used to create the adjacency matrix, transformation of adjacency matrix into a topological overlap matrix, and clustering of the topological overlap matrix using the cutreeDynamic function from WGCNA with method tree using a minimum module size of 10 as described previously.[38] Module significance was estimated using a permutation test as described previously.[38] Briefly, genes from the total list of genes used for module discovery were binned by expression, and 10 000 random modules with gene expression distributions like that of the tested module were generated. For each random module, a 1-sided Mann-Whitney *U* test was performed to compare the distribution of dissimilarity values between the tested module and the random module. The *P* values of these tests are corrected for multiple hypothesis correction with the Benjamini-Hochberg procedure, and the number of tests with false discovery rate >0.05 (indicating that the random module and tested module have similar dissimilarity distributions) was determined. If fewer than 5% of tests ($P<0.05$) fail to reject the null hypothesis of the Mann-Whitney *U* test, the tested module was deemed to have significant correlation structure relative to background.

Correlation and Scoring of Unsupervised Gene Modules Defining Antiproliferative Drug Response Across Shear Conditions

To determine whether significant correspondence existed between unsupervised gene modules identified from paclitaxel/rapamycin responses of high/low flow–conditioned cells, a Fisher exact test for significance of gene overlap was implemented. The significance of overlap size between each pair of modules was computed using the set of all differentially altered genes across both shear conditions as the gene universe. *P* values were adjusted using the Benjamini-Hochberg procedure. A score was computed for each WGCNA-based module for each cell as the total number of postnormalization transcripts (of the 10 000 normalized total) from genes in the module. These scores were scaled to *Z* scores based on the mean and SD across all cells.

Pseudotime Analysis

Single-cell trajectory analysis was conducted on RNA sequencing data using the Monocle 3 R package (version 3.3.9).[39] First, data were filtered based on drug conditions, and a standard preprocessing workflow was applied, including data normalization, selection of highly variable features, data scaling, and linear dimensional reduction, following previously described methods. To identify distinct cellular groups for each drug/flow condition, the Seurat package's FindNeighbors and FindClusters functions were used at different resolutions, ensuring at least 2 groups were discerned per condition. Uniform manifold approximation and projection was used as the nonlinear dimensional reduction technique for each drug condition.

To define the trajectory path, the learn_graph function from the Monocle package was utilized. Additionally, pseudotime computation and cell ordering were performed using the plot_cells and order_cells functions from Monocle, respectively.

Immunofluorescence Imaging

For immunofluorescence staining, flow was interrupted after 72 hours, and flow chambers were washed with PBS for 5 minutes. Cells were permeabilized with 0.1% Triton (Invitrogen). After 2× 10-minute washes, cells were blocked for 1 hour with 5% goat serum (Sigma-Aldrich) in PBS. The primary antibody was incubated overnight at 4 °C and washed 3× 10 minutes each before adding the secondary antibody for 2 hours at 37 °C. Cell Tracker (Invitrogen) and DAPI (Invitrogen) solutions were added after 3× 10-minute washes and incubated for 30 minutes. Following 3× 10-minute washes, cells were imaged for ki67 (Cell Signaling) expression in rapamycin-treated cells and α-tubulin (Cell Signaling) expression in paclitaxel-treated cells, and the morphology was evaluated based on the expression of DAPI and Cell Tracker with Cell Profiler (4.2.5).

RESULTS

Shear Stress Commits ECs to an Identifiable State

To understand EC dynamism defined by shear forces and understand cellular adaptation of ECs committed to well-differentiated controlled laminar flows, we used Seq-Well S^3 to characterize ≈5994 HAECs subjected to either high/physiological (30 dynes/cm^2) or low/altered (2.5 dynes/cm^2) laminar shear conditions in a controlled bioreactor system (Figure 1A; Figure S1). Following transcriptional profiling, dimensionality reduction was performed using PC analysis, and results were visualized with uniform manifold approximation and projection for dimension reduction, demonstrating that scRNA-seq profiles clearly resolved high and low shear-conditioned EC populations from each other (Figure 1B). The 3 shear replicates from each condition clustered together,

Downloaded from http://ahajournals.org by on July 13, 2026

Downloaded from http://ahajournals.org by on July 13, 2026

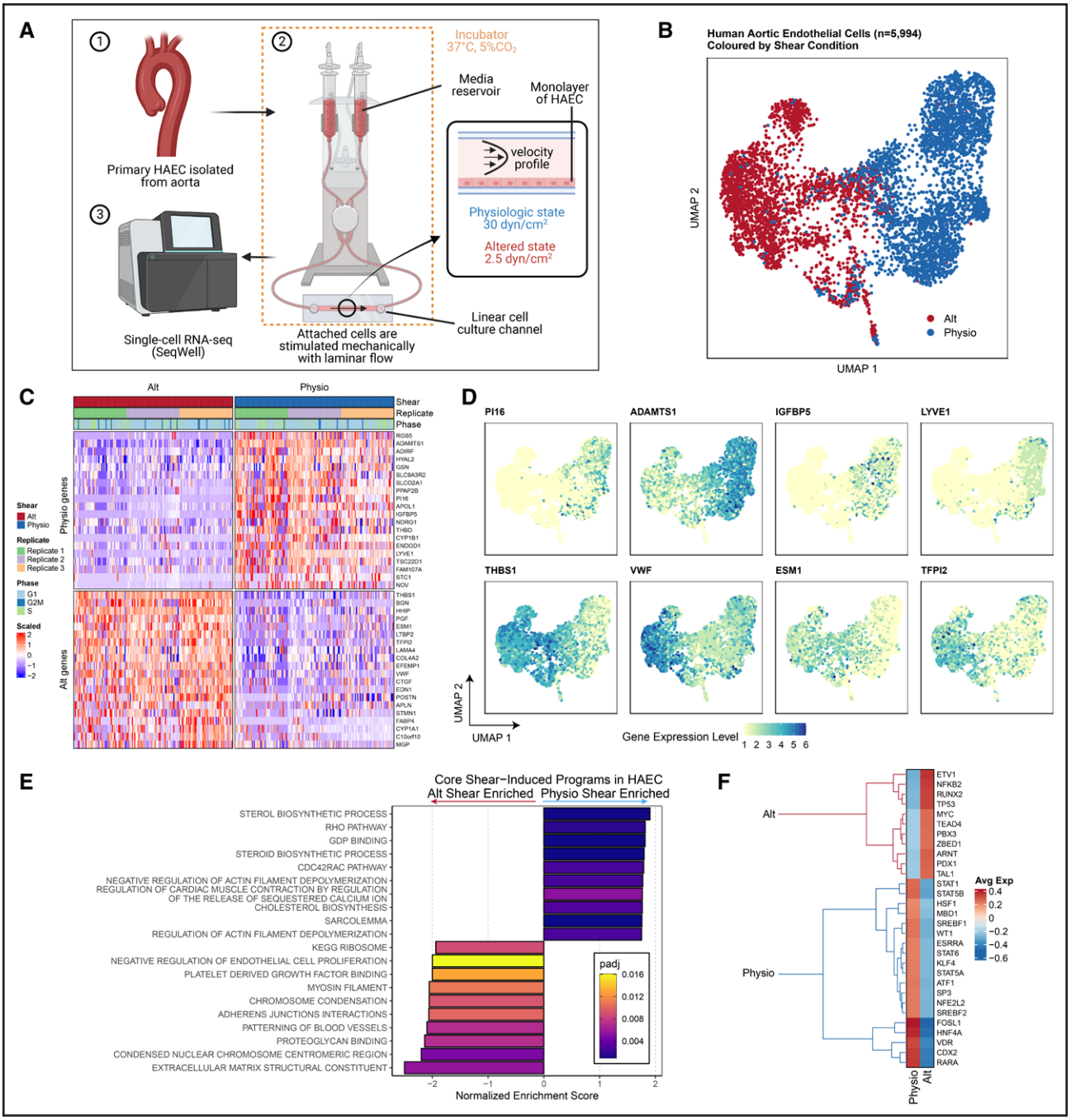

Figure 1. Shear forces determine the commitment of endothelial cells to distinct states.
A, Workflow for the stimulation of human aortic endothelial cells (HAECs) using a custom bioreactor system to control shear stress. Single-cell RNA sequencing (scRNA-seq) was used to assess transcriptional changes in HAECs subjected to high (30 dynes/cm^2) or low laminar flow–induced shear stress (2.5 dynes/cm^2). **B**, Uniform manifold approximation and projection (UMAP) visualization of 5994 HAECs from all samples (n=3). Cell types are color coded according to their respective shear states. **C**, Heatmap displaying the top 20 differentially expressed genes (DEGs) for each flow condition. **D**, Gene expression levels of 4 relevant markers for each flow condition, depicted in the UMAP. **E**, Visualization of gene set enrichment analysis results for different flow conditions. The color intensity of the bars represents the adjusted *P* value. **F**, Average expression of the top 30 transcription factors that discriminate between flow conditions.

demonstrating reproducibility of shear conditioning and transcriptional profiling independent of cell cycle phase (Figure S2A and S2B). DEGs of each shear condition were identified using the Wilcoxon rank-sum test as implemented in Seurat (Figure 1C). DEGs induced by high physiological shear include a number of genes that have previously been associated with high shear stress in HAECs and other human EC populations including PI16, a peptidase inhibitor[41]; ADAMTS1, a metalloproteinase[42]; IGFBP5, a mechanosensor in ECs[11]

(Figure 1D). LYVE1—typically considered a marker of lymphatic ECs—was also a DEG associated with high shear in this HAEC population. DEGs associated with low shear included THBS1, a thrombospondin[43]; VWF, a glycoprotein associated to hemostasis[44]; ESM1, EC secreted dermatan sulfate proteoglycan and related to inflammatory response[45]; and TFPI2, a serine protease inhibitor[46] (Figure 1D).

We then conducted shear-dependent GSEA using signature gene sets from the Canonical Pathways and Gene Ontology databases.[34] High laminar shear stress significantly upregulated (1) sterol biosynthesis, key in modulating biosynthesis of cholesterol and fatty acids[47]; (2) the Rho pathway, crucial in the regulation of cell morphology, proliferation, and adhesion[48]; and (3) regulation of actin filament depolarization, enabling turnover of actin filaments and cytoskeletal restructuring[49] (Figure 1E). These pathways are correlated with morphological changes observed in HAECs under immunofluorescence microcopy (Figure S3A and S3C). Top upregulated pathways in low laminar flow included extracellular matrix constituents, proteoglycan-binding pathways, and modulators of adherens junctions (Figure 1E). This GSEA confirms that the selected levels of shear stress in this study correspond to the 2 different regions in the set point theory that determines EC remodeling.[50]

Shear stress–induced TF activity was inferred using DoRothEA regulons[35] to partition shear-induced EC state (Figure 1F), allowing modular definition of shear-dependent states. TFs with activity upregulated in high laminar flow were associated with a wide range of EC functions, including, but not limited to, NO processing (KLF4[51]), redox response (NFE2L2[6]), vasculogenic and angiogenic processes (FOSL1[52] and HNF4α[53]), and blood pressure control (VDR[54]). TFs associated with low flow included NFKB2 (nuclear factor kappa B subunit 2), a mediator of inflammation with multiple links to thrombotic processes in ECs[55]; TP53, a regulator of EC dysfunction in hyperglycemia and ischemia[56]; and RUNX2, a mediator of EC migration and invasion during tumor angiogenesis.[57]

Single-cell profiling in combination with TF activity characterization enabled identification of biological associations among shear-responsive TFs in ECs (Figure 1F); for example, the HNF4α-FOSL1 activity was correlated, a relationship previously demonstrated in human colorectal cancer cells.[58] A relationship was also identified between retinoic acid and CDX family members (RARA-CDX2), a link previously found in vertebral patterning role through *Hox* gene expression.[59] The RUNX2-TP53 link identified in the study was found to mediate EC migration and invasion during tumor angiogenesis,[57] and a NFE2L2-SREBF2 interaction was previously found to regulate lipid metabolism.[60]

Taken together, the identification of shear-associated DEGs, shear-driven TF modules, and associations among these TF modules via single-cell profiling enabled a multitiered approach to characterization of shear-induced EC state in this model. Most importantly, analysis of DEGs and TF modules validated the physiological relevance of our in vitro model by recapitulating previously identified EC responses to shear stress, for example, the upregulation of KLF family members such as KLF2, KLF4, and KLF6 (Figure 1F; Figure S4D) in response to high physiological flow.

We additionally investigated the effects of turbulent flow in our bioreactor model. Within the vascular tree, atheroprone regions are known to be exposed to turbulent flow patterns accompanied by recirculation. To simulate this phenomenon, an oscillatory volumetric flow was deliberately induced in our turbulent flow model, resulting in the initiation of flow recirculation as demonstrated by computational fluid modeling (Figure S4A).

To comprehensively assess the impact of various flow conditions, we integrated transcriptional profiles of ECs subjected to both laminar and turbulent flow (Figure S4B and S4C). This endeavor revealed a significant overlap between turbulent flow conditions and the previously scrutinized high/physiological and low/altered-flow states. The coexistence of these conditions in turbulent areas of the vascular tree gives rise to EC heterogeneity and varying EC sensitivities to flow (Figure S4E). Moreover, these findings align consistently with the wall shear stress profiles derived from our computational fluid dynamic analysis (Figure S4A).

Notably, our investigation of the top DEGs influenced by shear stress (Figure 1C) further corroborates the convergence of turbulent flow conditions with the high and low shear stress phenotypes, with an overall average response lying between the high and low shear stress conditions (Figure S4D and S4E). Consequently, these genes hold promise as potential indicators to evaluate ECs' responsiveness to flow (Figure S4E), thereby validating their relevance in this context. Also, we demonstrated that the high and low laminar shear stress levels previously selected provide a distinct response to evaluate flow-sensitive transcriptional change in ECs and that turbulent flows with recirculation present a combination of both states.

Flow-Sensitive DEGs Discriminate Spatially Distributed EC Populations in Murine Aorta

Validation of DEGs and inferred TF profiles identified in this in vitro model was accomplished using previously described scRNA-seq profiles of ECs isolated from the murine aorta[21] (Figure 2A), which identified 3 spatially and functionally distinct EC subpopulations within the aortic vascular tree (Figure 2B). Subpopulations were previously differentiated by markers including VCAM1 and CD36 (Figure 2D) and thought to differ in aortic location; the VCAM1-positive EC1 group was localized to the aortic lesser curvature and the CD36-positive

Downloaded from http://ahajournals.org by on July 13, 2026

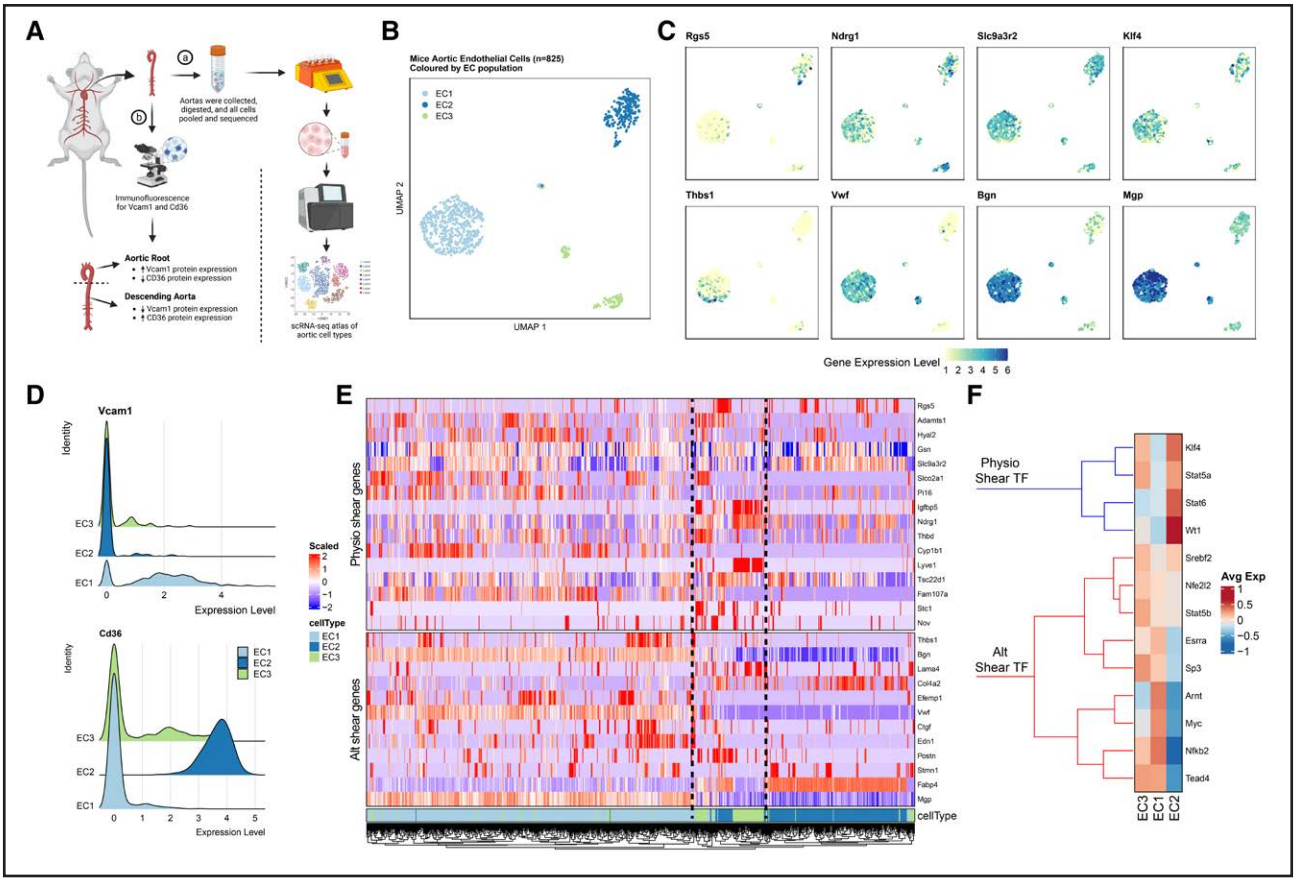

Figure 2. Shear-dependent genes reveal spatially distinct subpopulations of endothelial cells (ECs) in the murine aorta with distinct flow sensitivities.

A, Experimental methodology used by Kalluri et al[21] to isolate cell populations from the mouse aorta. Fluorescence microscopy demonstrated high VCAM1 and low CD36 fluorescence expression in the aortic root EC populations, while low VCAM1 and high CD36 fluorescence expression was observed in the descending aorta EC populations. **B**, Uniform manifold approximation and projection (UMAP) visualization identifying the 3 main EC clusters present in the mouse aorta. **C**, UMAP colored according to the expression of relevant shear-dependent differentially expressed genes (DEGs) identified in vitro using human aortic ECs (HAECs). **D**, Transcriptional expression levels of VCAM1 and CD36 in each EC subpopulation. **E**, Heatmap demonstrating how relevant shear-dependent DEGs identified in vitro using HAECs can characterize EC subpopulations in the mouse aorta. **F**, Correlation between shear-dependent TF (transcription factor) response in the mouse aorta and the TF response observed in HAECs.

EC2 group to the greater curvature and descending aorta.

The top DEGs influenced by flow shear stress in the in vitro model (Figure 1C) were sufficient to discriminate these 3 in vivo subpopulations previously identified using the entire transcriptome (Figure 2B and 2E). EC1 and EC3 subpopulations exhibited higher overall sensitivity to flow, with an upregulation of shear stress–sensitive genes compared with EC2 (Figure 2E). Moreover, EC1 and EC3 demonstrated less expressions of high shear–related genes, such as *RGS5* (regulation of G protein signaling 5), *NDRG1*, *SLC9A3R2*, and *KLF4*, but greater expression of low shear–related genes, such as *THBS1*, *VVF*, *BGN*, and *MGP* (Figure 2C). This finding aligns with the idea that the low shear stress level defined in our in vitro experiment correlates with regions of recirculation or aberrant flow, where atheroprone regions are found within the vascular tree. Furthermore, analysis of the inferred TF modules defined using the flow loop bioreactor in the in vivo data revealed an upregulation of low/altered shear–related TFs in the EC1 subpopulation, such as NFKB2, ARNT, MYC, or TEAD4, while EC2 predominantly overexpressed the high/physiological shear-related TFs identified in our in vitro data, such as KLF4, STAT5, STAT6, or WT1 (Figures 1F and 2F).

The inferred TF module analysis on murine data revealed that some previously defined in vitro biological associations correlated with in vivo findings (Figures 1F and 2F). For instance, the NFE2L2-SREBF2 interaction may be involved in the regulation of oxidative stress and lipid metabolism, both of which were affected by the response of ECs to flow shear stress in our GSEA (Figure 1E). Another relationship found in both data sets was WT1 and STAT6, which may play a role in EC development, inflammation, or immune response and share common or parallel pathways in the regulation of NO production and inflammation mediated by the

Downloaded from http://ahajournals.org by on July 13, 2026

mechanotransduction response of ECs to shear stress. STAT5B, ESRRA, SP3, and NFE2L2 were identified as low shear–related TFs in both in vitro and in vivo analyses, and they may share signaling pathways with the response of ECs to shear stress through their role in the regulation of the immune system, energy metabolism, and oxidative stress response. Finally, MYC, TEAD4, and ARNT were associated with high/physiological shear stress–related TFs, and their roles in regulating EC proliferation, development, and environmental signaling may be linked to the EC signaling pathways activated by ECs in response to physiological shear stress to maintain vascular homeostasis.

Antiproliferative Therapies Elicit Unique EC Fingerprints When Costimulated With Distinct Flow Conditions

To build on our results in EC populations responding to a single stimulus, we used scRNA-seq to profile ≈6252 HAECs cultured in a bimodal stress experiment under high/physiological or low/altered laminar flow (as defined previously) with or without administration of antiproliferative therapies (Figure S1). This experiment resembles endovascular treatment scenarios where ECs are first committed to high or low levels of shear stress at the endothelium wall by local anatomy and pathology. In the course of clinical treatment, antiproliferative drugs are released by diffusion from a drug-eluting stent/balloon. Given the broad known effects of rapamycin and paclitaxel on EC proliferation and migration,[13,61] calcium dynamics,[14,62] and autophagy,[18,63] as well as impact on flow-responsive elements like KLF2[17] (rapamycin), their effects in this system were defined both independently of and in combination with shear alteration. For shear-independent analysis, drug effects were evaluated irrespective of shear stress level. Drug concentrations selected in this work have been previously demonstrated to result in alterations in RNA expression in ECs.[17,27] Dimensional reduction with PC analysis and visualization with uniform manifold approximation and projection demonstrated clear resolution of cell populations by shear condition and clear resolution of the rapamycin/paclitaxel-treated population under high shear stress conditions but not in low shear stress conditions for rapamycin-treated cells (Figure 3A and 3D).

First, the response elicited by antiproliferative therapies was analyzed independently of shear-induced state. DEGs upregulated by paclitaxel were involved mainly in encoding heterodimers of α/β-tubulins and microtubules (TUBB2A, TUBA1A, TUBA1B, TUBB, and MAP2), modulating cholesterol biosynthesis (MSMO1), and regulating autophagy (ATF4; Figure 3B and 3C). DEGs downregulated by paclitaxel include those previously found in high shear-dependent genes such as *ADAMTS1*, *IGFBP5*, *THBD*, *RGS5*, and *HYAL2* (Figure 3C). GSEA confirmed primary pathways activated by paclitaxel were related to sterol biosynthesis and tubulin formation (Figure 3G). Primary pathways negatively enriched by paclitaxel included regulation of EC plasma membrane, such as ankyrin and integrin binding (Figure 3G). Overall, paclitaxel impacts genes related to cell function and vascular integrity (EMCN, by stabilizing the EC barrier and modulating vascular permeability[64]; SCD, through lipid metabolism[65]), cell division, cellular intracellular transport, and maintaining cell shape (TUBA1B, TUBB, TUBA1A, and TUBB2A, major members of microtubules of the cytoskeleton[66]; MAP2, stabilizing microtubules[67]), apoptosis (ATF4, by modulating amino acid metabolism and antioxidant responses[68]), and cell proliferation (MALAT1, a long noncoding RNA regulating the expression of other genes[69]). We substantiated the influence of paclitaxel at the protein level through an analysis of its effects on α-tubulin. Our observations revealed a significant alteration in cell morphology induced by paclitaxel, regardless of whether the cells were subjected to physiological or altered-flow conditions (Figure S3C, S3D, and S3F).

The EC response to rapamycin independent of shear state revealed upregulated DEGs involved in the regulation of kinase A (AKAP12), cell differentiation and proliferation (HMGA1, NDRG1, and IGFBP5), and calcium dynamics (S100A6; Figure 3E and 3F). Downregulated DEGs by rapamycin included POSTN, which regulates tissue regeneration and wound healing through cell attachment; GJA4 and GJA5, which encode gap junction proteins; and HSPA5 and HSP90B1, which are key in protein folding and stabilization (Figure 3F). GSEA revealed that the main effect of rapamycin in ECs is to repress multiple biological pathways, including regulation of proteasomes, protein folding, angiogenesis, and calcium ion channels (Figure 3H). Overall, rapamycin impacts genes related to cell migration and adhesion processes (LMO7, via regulation of scaffolding/cytoskeletal organization[70]), cell proliferation (S100A6, by regulating calcium-binding proteins[71]; NDRG1 and SERPINB1, well-known tumor suppressors[72,73]; HMGA1, a chromatin-binding protein modulating transcription of various genes[74]), and endothelial permeability (CLDN5, through tight junction expression[75]). The impact of rapamycin on HAECs was additionally examined at the protein level, assessing its influence on proliferation by observing the ki67 expression (Figure S3B and S3E). Our findings demonstrate that rapamycin effectively regulates HAEC proliferation at both the transcriptomic and protein levels, leading to a notable reduction in ki67 expression, regardless of the prevailing flow conditions.

EC Cellular Adaptation to Antiproliferative Therapies Is Altered by Flow-Induced Shear Stress

The combined response of shear forces and antiproliferative therapies was analyzed by first computing a

Downloaded from http://ahajournals.org by on July 13, 2026

Downloaded from http://ahajournals.org by on July 13, 2026

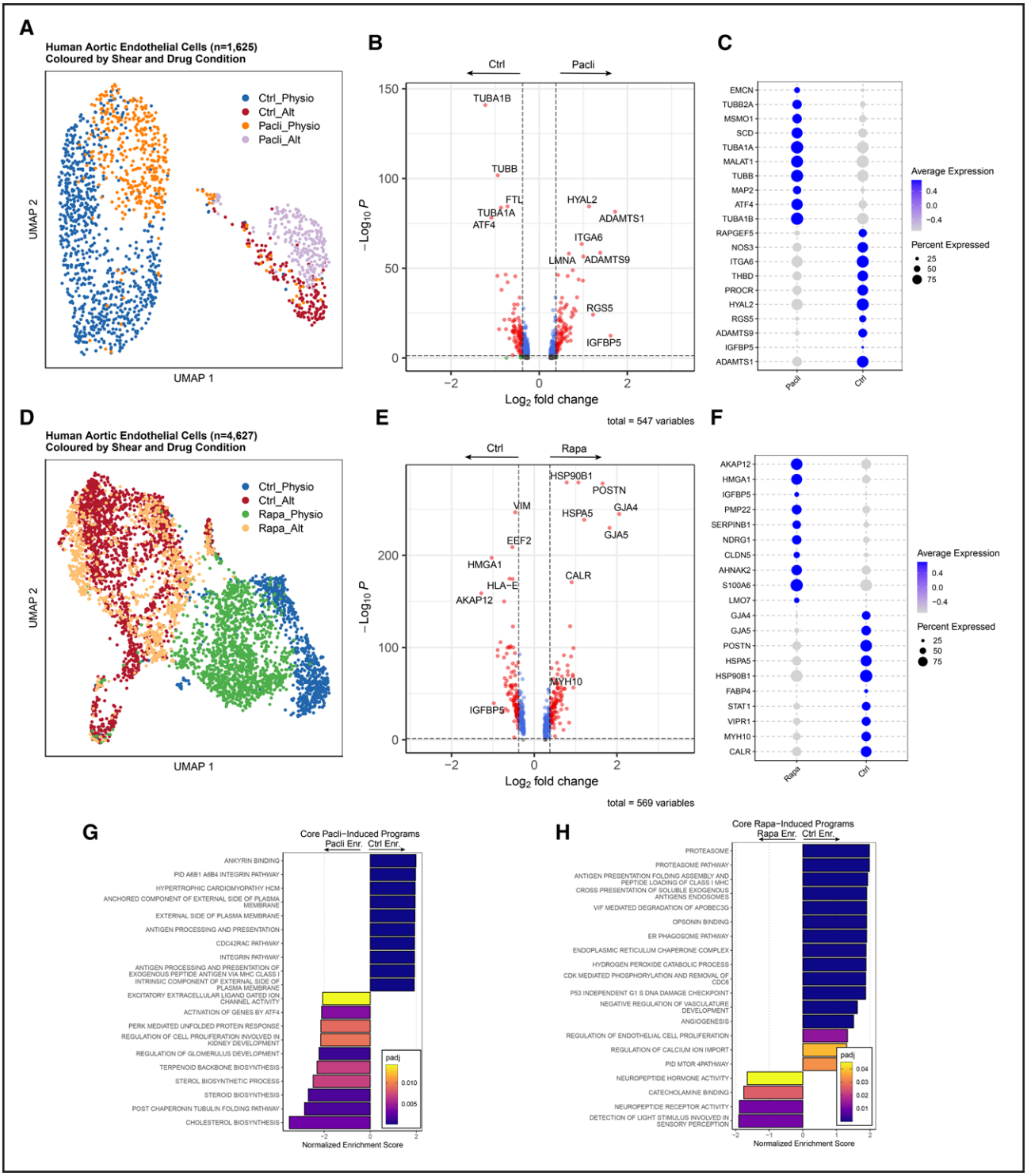

Figure 3. Antiproliferative therapies induce a distinctive signature in endothelial cells (ECs) when costimulated with different laminar flows.

A, Uniform manifold approximation and projection (UMAP) visualization of 1625 human aortic ECs (HAECs) stimulated with shear forces and paclitaxel. Cell types are labeled with colors corresponding to the shear flow and drug states. **B**, Volcano plot illustrating the top differentially expressed genes (DEGs) upregulated or downregulated by paclitaxel when ECs are exposed to any flow condition. **C**, Dot plot summarizing the top 10 genes upregulated or downregulated by the drug condition (paclitaxel). **D**, UMAP visualization of 4627 HAECs stimulated with shear forces and rapamycin. **E**, Volcano plot illustrating the top DEGs upregulated or downregulated by rapamycin when ECs are exposed to any flow condition. **F**, Dot plot summarizing the top 10 genes upregulated or downregulated by the drug condition (rapamycin). **G**, Visualization of the gene set enrichment analysis for paclitaxel independent of flow condition. The color intensity of the bars represents the adjusted *P* value obtained from gene set enrichment analysis (GSEA). **H**, Visualization of the gene set enrichment analysis for rapamycin independent of flow condition.

hierarchical clustering of single-cell profiles based on a Euclidean distance matrix. A single heatmap was used to represent the response induced by flow state and either paclitaxel (Figure 4A) or rapamycin (Figure 4C). Identifiable shear states are denoted in both therapies, with drug stimulation clearly displaying a unique fingerprint in ECs when costimulated with high shear stress conditions (Figure 4A and 4C). However, the pharmacological response is more limited in low shear stress states, in which the single-cell transcriptional profile cannot differentiate cells stimulated with antiproliferative drugs from control cells (Figure 4A and 4C).

Limitation of EC response to antiproliferative therapy when exposed to altered shear stress was corroborated using trajectory-based differential expression analysis. Subclusters defining EC heterogeneity within flow/drug groups (Figure S8A through S8E and S8H through S8L) were subjected to trajectory analysis, with the dominant pseudotime coordinate primarily driven by the sensitivity of ECs to flow-induced shear stress both in rapamycin

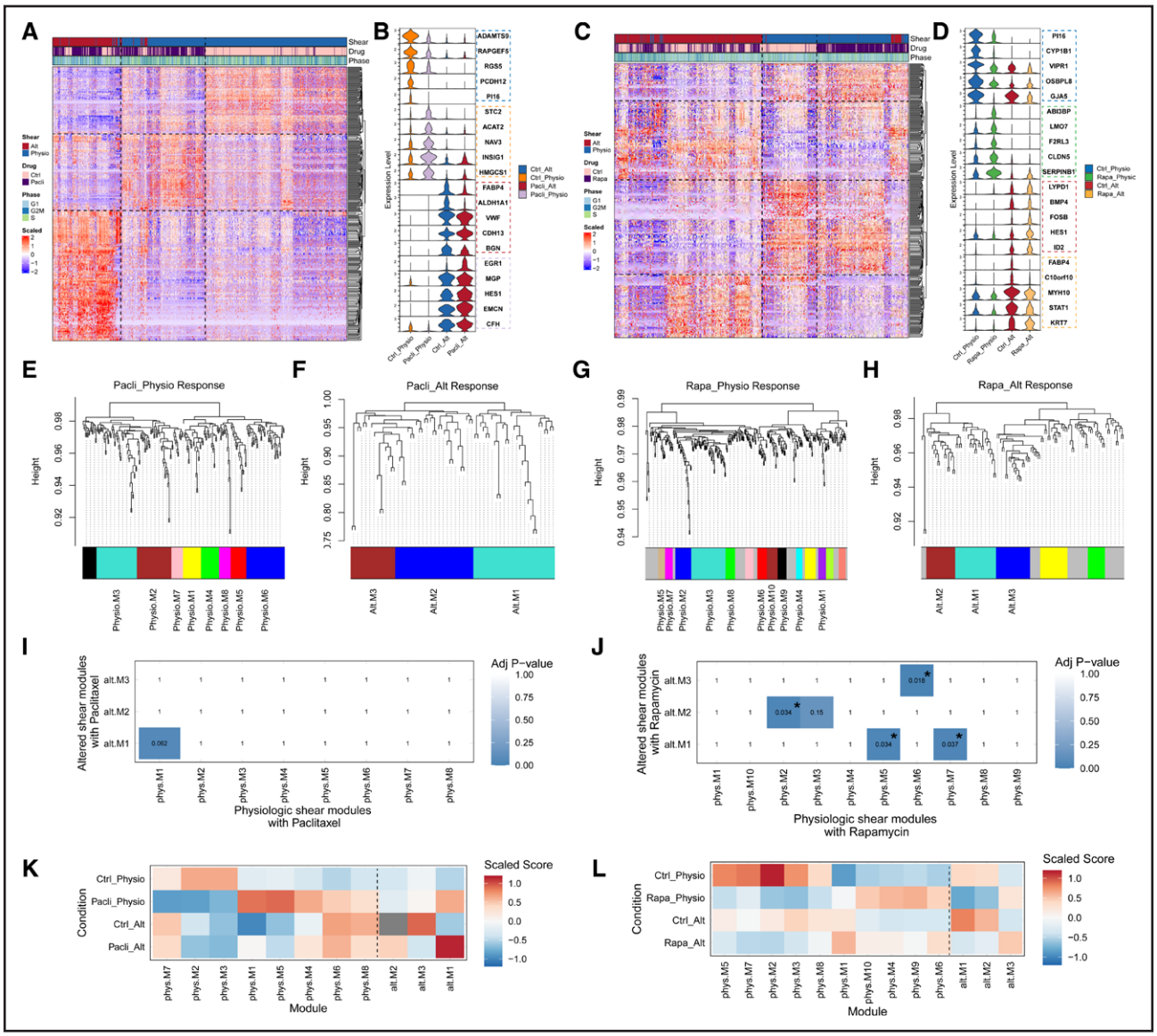

Figure 4. Shear stress influences the cellular response of endothelial cells to antiproliferative drugs.
A, Hierarchical heatmap displaying the Euclidean distances between differentially expressed genes (DEGs) and cells costimulated with paclitaxel. **B**, Gene expression levels of 5 relevant markers for each flow/paclitaxel condition. **C**, Hierarchical heatmap showing the Euclidean distances between DEGs and cells costimulated with rapamycin. **D**, Gene expression levels of 5 relevant markers for each flow/rapamycin condition. **E** through **H**, Weighted gene correlation network analysis (WGCNA) applied to DEGs in high and low shear stress conditions with paclitaxel or rapamycin. Candidate gene modules of minimum size are identified with colored bars, and gene modules with significant intramodule correlation strength are labeled. **I** and **J**, Identification of corresponding modules in high and low shear stress conditions using overlap significance testing. **K** and **L**, Mean WGCNA-based module scores for each experimental condition, scaled and centered across all cells. Ctrl, control condition (high or low shear stress state without drug); High, high shear stress (30 dynes/cm^2); Low, low shear stress (2.5 dynes/cm^2); Pacli, paclitaxel stimulation; and Rapa, rapamycin stimulation.

Downloaded from http://ahajournals.org by on July 13, 2026

Downloaded from http://ahajournals.org by on July 13, 2026

and paclitaxel-exposed cells (Figure S8F and S8M). Furthermore, we found that ECs have a higher sensitivity to antiproliferative drugs when exposed to high/physiological flows rather than low/altered flows, showing a more significant difference in the average pseudotime response in the presence of high/physiological shear stress (Figure S8F and S8M).

Relevant DEGs were identified for each flow/drug condition (Figure 4B and 4D). DEGs upregulated by high shear stress or downregulated by paclitaxel are involved in cleavage of proteoglycans (ADAMTS9), RGS5, and modulating cellular adhesion (PCDH12). Cholesterol biosynthesis (MHGCS1, INSIG1, and ACAT2) and autocrine/paracrine signaling modulation through action on calcium and phosphate ions were related to paclitaxel response in high laminar flow shear stress state (STC2). Few DEGs offered a unique response to identify paclitaxel stimulation in the low shear stress state. To further validate the relevance of these DEGs, pseudotime trajectory analysis revealed significant changes in pseudotime response for ACAT2, ADAMTS9, INSIG1, PCDH12, RGS5, and STC2 in paclitaxel-treated HAECs in the presence of flow (Figure S8G).

Pseudotime trajectory analysis further validates the fluctuations experienced by DEGs in response to both flow shear stress and rapamycin, showing a higher relative expression change in the regions where the pseudotime corresponds to high/physiological flow and rapamycin-treated HAECs (Figure S8N). Altogether, these findings reveal that EC cellular adaptation depends primarily on shear stress levels. More specifically, in low-flow shear stress states, the EC cellular adaptation to chemical stimuli has been diminished, limiting the response to antiproliferative drugs.

To leverage the ability of scRNA-seq to further dissect the components of EC dynamism in response to antiproliferative therapies in an unbiased fashion, a previously described unsupervised WGCNA-based method coupled with a significance test[38] was used to identify coexpressed gene modules consisting of at least 10 genes in the response of flow-conditioned ECs to paclitaxel/rapamycin. The paclitaxel/rapamycin response under high shear stress was defined as the set of DEGs between the high shear stress cells with drug and the high shear stress cells without drug, which consisted of 244 genes in paclitaxel-stimulated cells and 324 genes in rapamycin-stimulated cells (Figure S5C). The paclitaxel/rapamycin response under low shear stress was defined as the set of DEGs between the low shear stress cells with and without drugs, consisting of 66 genes in paclitaxel-stimulated cells and 137 genes in rapamycin-stimulated cells (Figure S5C). Of note, in both cases, the high flow-conditioned drug response consisted of more total genes than the low flow–conditioned drug response. The WGCNA-based module identification and significance testing procedure was applied separately to both sets. This process identified 8 distinct coexpressed modules of at least 10 genes in the high shear stress condition and only 3 modules in the low shear stress condition in cells stimulated with paclitaxel (Figure 4E and 4F). For rapamycin-stimulated cells, 10 modules were found in high flow and 3 modules under low flow. (Figure 4G and 4H). Overall, fewer DEGs and WGCNA-derived modules were found in low flow conditions in either paclitaxel or rapamycin-stimulated cells, showing a reduced complexity of antiproliferative drug response in low shear–conditioned ECs.

The coexpressed transcriptional modules comprising the response of high shear–cultured HAECs to paclitaxel included a tubulin/cytoskeleton assembly and rearrangement set including TUB family genes (TUBA1B, TUBB, TUBA1A, TUBB2A, TUBB6, and TUBA1C), which clearly correlates with changes in the α-tubulin protein expression, modifications in the cell cytoskeleton, and overall morphology when HAECs are exposed to paclitaxel, both under high and low shear stress conditions, which were not observed when cells were treated only with rapamycin (Figure S3C, S3D, and S3F); a blood vessel morphogenesis set including ADAMTS1 and THBD; a cell adhesion and migration/locomotion set, including platelet and EC adhesion molecules (PECAM1) and integrins (ITGA6 and ITGB4); a supramolecular complex and tubulin/cytoskeleton complex set, including microtubule-associated proteins (MAP2); a sterol metabolic/biosynthetic process set including several enzyme coding proteins such as reductases (HMGCR, DHCR7, and DHCR24) or isomerases (IDI1 and EBP); a ribosome/cytoplasmic translation set, including ribosomal proteins (eg, RPL41 and RPL27); a tube development/morphogenesis set and one unannotated gene set without known functional gene enrichment including KLF6, SERPINE2, and ANKRD1 (Table S1). Coexpressed transcriptional modules comprising the simpler response of EC culture under low shear stress and paclitaxel included a tubulin/cytoskeleton assembly a rearrangement set, an extracellular matrix/cell surface set, and a cell adhesion set (Table S2). Twenty-three genes were present in both the high shear response modules and the low shear response modules. Of these, 7 were members of the respective tubulin/cytoskeleton assembly and arrangement modules (High.M1 and Low.M1). Notably, the remainder were distributed among both the other low shear–response modules, but 2 high shear–response modules (High.M3 and High.M7) included no common genes.

Similar analysis was performed on rapamycin data, with the coexpressed transcriptional modules comprising the response of high shear–cultured ECs to rapamycin including an extracellular matrix/cell surface molecule set with GJA4 and GJA5 molecules; a cell adhesion/migration set including TMEM100 and BMPER; an endoplasmic reticulum/antigen processing set including

Downloaded from http://ahajournals.org by on July 13, 2026

B2M, CALR, and PDIA3; a vasculature development set including TUBB; a peptide/ribosomal synthesis gene set; 2 additional segregated sets also related to cell adhesion and endoplasmic reticulum processing; and a mixed set enriched mainly for regulation of protein metabolic process but including mechanotransduction genes such as *PIEZO2*. Two unannotated gene sets without known functional gene enrichments included an IL-33/COL1A2/SNX3 module and a PLXNA2/TUBA1C/SLC26A2 module (Table S3). All these modules affecting cell adhesion, extracellular matrix development, and cell migration are indirectly correlated with the well-known effect of rapamycin on cell proliferation, as it affects the cell cycle. These effects are relevant in both high/physiological and low/altered shear stress conditions, as evidenced by the diminished expression of ki67 when cells are treated with rapamycin (Figure S3B and S3E). Coexpressed transcriptional modules comprising the simpler response of ECs cultured under low shear stress and rapamycin included a peptide/ribosomal synthesis gene set, an endoplasmic reticulum processing gene set including CALR, PDIA6, and MMP14, and cell anchoring/junction organization set including GJA4 and GJA5. Thirty genes were present in both the high shear response modules and the low shear response modules (Table S4). Of these, 13 were members of the low shear endoplasmic reticulum model modules (Low.M1) and equally divided in the respective high shear modules (High.M5 and High.M7); and 12 were members of the low shear cell anchoring/junction organization module (Low.M2) and unevenly divided in the respective high shear module (10 genes in High.M3). The remainder were distributed among both the other low shear response modules but 4 high shear response modules included no common genes (High.M1, High.M4, High.M9, and High.M10).

To use this method of decomposing the EC cellular adaptation to paclitaxel/rapamycin to understand the effect of shear on drug response, we identified significant overlaps between the modules from each shear condition with the goal of functionally linking modules under both conditions (Figure 4I and 4J). No significant linkages were identified in the paclitaxel data set. The tubulin/cytoskeleton assembly and rearrangement modules, main paclitaxel targets, showed a substantial but nonsignificant overlap in each flow state. Notably, the remaining modules of paclitaxel-stimulated cells (Low.M2 and Low.M3) present in the low shear set had no significant overlaps with multiple modules in the high shear paclitaxel response, including the blood vessel morphogenesis module, the cell adhesion and migration/locomotion module, and the tube development/morphogenesis module. Regarding rapamycin-stimulated cells, a significant overlap was present between the endoplasmic reticulum processing module of the 2 flow responses, as well as with the cell anchoring/junction organization set. Another group with strong correspondence in both flow conditions was peptide/ribosomal synthesis gene sets. A weaker overlap was also present between the cell anchoring/junction organization module in the low shear state and the cell adhesion/migration module in the high shear state.

The differences between the high and low shear responses to paclitaxel/rapamycin were further clarified by scoring expression of each module across all cells and examining differences in mean scores among shear conditions (Figure 4K and 4L). In general, rapamycin-induced changes in the modules identified under high shear were blunted under low shear stress, while changes in the modules identified under low shear had similar magnitude in both conditions (Figure 4L). Paclitaxel-induced changes under high shear were also blunted under low shear stress, but changes identified under low shear had either a similar magnitude in both conditions or were significantly decreased in high conditions (Figure 4K). In addition to the mean scores, score distributions were examined across conditions (Figures S6 and S7). Unsurprisingly, the addition of paclitaxel/rapamycin resulted in a significant change in expression of all modules in both shear conditions. However, most of the modules first identified via the paclitaxel/rapamycin response were also significantly altered by shear alone, in keeping with the interrelation of the 2 stimuli.

Finally, we contrasted the combined response of paclitaxel and rapamycin under both high and low shear stress conditions (Figure S5A and S5B). As expected, there were only a few common DEGs in the different flow conditions treated with these antiproliferative mechanisms (Figure S5C). Most of the relevant DEGs showed different expression levels for each drug/flow condition (Figure S5E) due to their distinct mechanisms of action: rapamycin inhibits the mTORC1 complex, leading to cell cycle arrest at the G1 phase, while paclitaxel binds and stabilizes microtubules, resulting in cell arrest in the mitotic phase.

Unsurprisingly, many of the regulated programs revealed with gene enrichment were mainly driven by TUBB family genes (Figure S5D), which encode β-tubulin proteins crucial for microtubules, the target of paclitaxel, and indirectly affected by rapamycin due to the mTOR pathway's influence on microtubule dynamics as a downstream effector when regulating cell metabolism, proliferation, and growth.

DISCUSSION

Understanding EC cellular adaptation is fundamental to understanding the regulation of blood vessel homeostasis. ECs are exposed to multiple categories of stressors that alter the homeostatic quiescent state of the healthy, intact endothelium. Therefore, elucidating EC cellular adaptation in response to discrete stressors is a requirement for further advances in vascular biomedicine, from

finding novel biomarkers for cardiovascular disease prognosis to explaining the high variability in endovascular interventional outcomes for cardiovascular disease. Here, we use scRNA-seq to profile HAEC populations subjected to differing shear stresses found in the human aorta as a paradigmatic mechanical stimulus, both alone and in combination with antiproliferative agents as paradigmatic chemical stimuli. Our results enable definition of EC capacity to respond to these environmental factors with single-cell resolution, which in turn provides new insights into the transcriptional modules comprising the EC state, as well as the coupling among these modules that gives rise to functional cellular adaptation in the context of environmental stimuli singly or in combination. Our results demonstrate the following advances in the study of EC functional dynamism: (1) shear- and drug-induced states can be defined with high resolution via the single-cell EC transcriptome; (2) shear-induced EC states correspond to previously identified in vivo EC heterogeneity; (3) shear stress modulates the EC adaptation to other stimuli; and (4) the low/altered shear-induced EC state limits the complexity of the response to widely used pharmacological regulation. ECs committed to respond to low shear, as found in the atheroprone regions of the aorta, have a reduced ability to alter their state in response to pharmacology, here, to the chief classes of drugs used in vasoactive implants (ie, paclitaxel and rapamycin).

The understanding of changes induced by shear stress has evolved over decades as the linchpin of investigations into the EC state.[7] At a population level, our transcriptional profile demonstrates a generalized increase in the expression of ribosomal and mitochondrial transcripts under low shear stress (Figure S2C and S2D). Low shear stress induces endoplasmic reticulum stress and the related unfolded protein response pathway.[9] Typically, activation of the unfolded protein response is associated with translational repression, making the association of low shear with ribosomal transcript upregulation in our data set surprising; however, a distinct feedback arm in the unfolded protein response mediated by ATF4 and GADD34 has the effect of restoring protein synthesis and is linked to ribosomal biogenesis via NMP4.[76] This is particularly relevant in the setting of long-term endoplasmic reticulum stress, as might be expected during the multiday bioreactor model of shear conditioning used in this study.[77] The increase in mitochondrial transcripts may be partially explained by the previous suggestion that mitochondrial biogenesis is protective against endoplasmic reticulum stress.[78]

A value of extending the characterization of shear-induced EC state to the single-cell level is in placing previous results in context by identifying the top TF-based programs that are most important for defining shear state and to enable investigation of how they are coupled to each other across a population of ECs. Given the complex and multifactorial drivers of the EC state, we accomplished this by conceptualizing shear-driven EC state as the combination of multiple TFs for each flow condition (Figure 1F). Our results demonstrate that a relatively small number of TFs based on their shear-responsive activity can capture shear-induced state sufficiently to differentiate shear-induced states. Although these top TFs do not include the full complexity of the original scRNA-seq profiles, they serve as an interpretable bridge between the complete transcriptome and prior knowledge on shear-responsive elements in ECs. This analysis enables direct comparison of TF modules to determine which factors are most important for definition of shear stress–induced state. FOSL1, HNF4A, VDR, CDX2, and RARA were most important for defining high shear–induced state, while ETV1, NFKB2, RUNX2, and TP53 were the greatest contributors to low shear–induced identity. Understanding endothelial dynamism from the perspective of discrete TFs with single-cell resolution enables a middle ground between the traditional model of dysfunctional or activated endothelium and the molecular biology of individual pathways. This same paradigm can be used to characterize EC adaptation in response to a variety of metabolic stressors in terms of shifts in the network of coupled TF-based activity.

Our single-cell transcriptional profiling also demonstrated that the components of shear state are not all expressed in the same cells but are instead upregulated differentially among different shear-cultured HAECs, as observed previously in human umbilical vein ECs.[25] This suggests that the endothelial response to shear stress is not monolithic but instead consists of distinct but correlated transcriptional programs, which may be linked to distinct phases or degrees of shear response in combination with other stimuli, as evaluated in our pseudotime analysis. This heterogeneity has been further investigated as a potential origin of spatial EC heterogeneity observed in vivo,[21] revealing well-localized EC subpopulations in the aorta expressing different flow sensitivities. The top flow-sensitive DEGs and TFs found here in vitro enabled the identification of EC subclusters previously defined in vivo.

The components of the endothelial response to antiproliferative drugs are much less well described than those comprising the response to shear stress, although they have been linked to multiple effects on endothelial processes including migration and proliferation.[14] From a population perspective, our data on the response of high shear–cultured ECs to paclitaxel and rapamycin provide new insight into their effects on EC functional phenotype, including changes in the expression of transcripts implicated in sterol biosynthesis, tubulin formation and vasculature development in paclitaxel-stimulated cells and endoplasmic reticulum handling, cell adhesion/anchoring, and angiogenesis in rapamycin-stimulated cells. Intriguingly, exposure to low shear stress limits the antiangiogenic potential of both paclitaxel and

Downloaded from http://ahajournals.org by on July 13, 2026

rapamycin on ECs as identified here both by gene set enrichment on high shear–specific paclitaxel/rapamycin response genes and by identifying discordant genes in corresponding paclitaxel/rapamycin response modules under differing shear conditions. Functional analyses of this type are necessary to understand high-resolution transcriptional data in terms of implications for vascular pathology and therapy. Thus, transcriptional profiling of this type enables both new understanding of the functional effects of a complex multifactorial stimulus and how these effects are modulated by additional stressors.

As with shear stress alone, the characterization of drug (paclitaxel/rapamycin)-exposed populations with single-cell resolution enabled identification of discrete transcriptional modules as components of EC adaptation. ECs subjected to high shear had a more complex response to antiproliferative drugs, consisting not only of more DEGs but also with more distinct transcriptional modules with significant correlation among component genes. Many of the modules identified in the response of high shear–conditioned ECs corresponded to the major EC functions identified in the bulk response, while others had no clearly enriched function. By contrast, the response of low shear–conditioned ECs to antiproliferative drugs consisted of fewer genes with fewer distinct modules with less well-defined functions, with a notably blunted response in genes associated with angiogenesis, vasculature development, or cell migration. In rapamycin-exposed cells, the endoplasmic reticulum–based module in the high shear–exposed cells notably included certain homeostatic functions such as antigen processing, which were lost in the low shear modules, possibly due to engagement of endoplasmic reticulum machinery by low shear–induced unfolded protein response. This result has an important implication for our understanding of stimulus-driven EC functional heterogeneity—namely, that the response to one external stimulus can limit the metabolic response to a second stimulus (rapamycin). Dysfunctional EC processes including endoplasmic reticulum stress and the unfolded protein response may represent forcing states, which dampen shifts driven by other stimuli. This is a vital consideration for the development and understanding of other vasoactive therapeutics, which as a rule are deployed in the context of endothelium already made dysfunctional with vascular disease. This method for module-based understanding of EC adaptation can also be utilized for other combinatorial stimuli—whether pharmacological or pathological—with complex effects on ECs that are as yet poorly understood.

Our study has shed light on the effects of single doses of antiproliferative agents on transcriptional changes in ECs, as well as the impact on proliferation and cytoskeletal protein function. However, it is essential to acknowledge the limitations that may influence the interpretation of our findings. First, the use of a single dose for each agent, while validated for inducing significant changes, may warrant further investigation with multiple doses to strengthen the robustness of our conclusions. Second, though 3 replicates were included to enhance reliability, the lack of access to the genetic backgrounds of donors may limit the generalizability of our results, especially when studying populations with diverse genetic backgrounds. Third, many of the transcriptional programs identified in this work as responsive to flow and antiproliferative drugs include substantial posttranscriptional components, which must be investigated in future work applying proteomic and functional assays. Despite these limitations, our research provides valuable insights and highlights the EC sensibility to flow and the altered capacity of EC to respond to antiproliferative treatments when cells are committed to distinct pathophysiological flows.

In conclusion, we present here the use of scRNA-seq to profile EC populations subjected to controlled external stimuli singly and in combination to elucidate the distinct components of EC cellular adaptation. We demonstrate how shear stress limits EC response to other stimuli, including antiproliferative drugs delivered during endovascular treatments. ECs are above all environmentally sensitive cells, especially driven by flow and flow-induced shear stress, and serve to discern distinct EC subpopulations is the aorta. As such, it seems that once exposed to flow alterations, ECs commit to responding to this stress state, altering their capacity to remain responsive to subsequent stresses, for example, chemical exposures. Continued understanding of the function and dysfunction of distinct endothelial subpopulations and their potential response to vasoactive therapeutics will depend on continued utilization of these techniques for probing ECs, especially at the protein level.

ARTICLE INFORMATION

Received March 10, 2023; accepted September 7, 2023.

Affiliations

Institute for Medical Engineering and Science (A.G.S.-M., A.S.K., M.A.V., T.K.H., M.H.W., T.T.D., M.B., A.K.S., E.R.E.) and Koch Institute for Integrative Cancer Research (T.K.H., M.H.W., A.K.S., E.R.E.), Massachusetts Institute of Technology (MIT), Cambridge, MA. Broad Institute of MIT and Harvard, Cambridge, MA (A.G.S.-M., M.A.V., T.T.D., A.K.S.). Ragon Institute of MGH, MIT, and Harvard, Cambridge, MA (M.A.V., T.K.H., M.H.W., T.T.D., A.K.S.). Departments of Biology (M.A.V.), Biological Engineering (T.T.D.), and Chemistry (A.K.S.), Massachusetts Institute of Technology, Cambridge. Department of Immunology, Harvard Medical School, Boston, MA (T.K.H., M.H.W., A.K.S.). Division of Cardiac Surgery (F.R.N.) and Division of Cardiovascular Medicine, Department of Medicine (E.R.E.), Brigham and Women's Hospital, Boston, MA.

Sources of Funding

A.G. Salazar-Martín received the support of a fellowship from La Caixa Foundation (ID 100010434; LCF/BQ/AA1 9/11720044) and the MathWorks Engineering Fellowship. These fellowships were used to support his PhD studies at the Harvard/Massachusetts Institute of Technology (MIT) Medical Engineering and Medical Physics Program. A.S. Kalluri was supported by the National Institutes of Health (NIH) National Institute of General Medical Sciences via grants to the Harvard/MIT Medical Scientists Training Program and the Harvard Biophysics Program (T32GM007753 and T32GM008313), as well as the American Heart Association Predoctoral Fellowship (18PRE34060009). A.K. Shalek was supported by the Searle Scholars Program, the Beckman Young Investigator Program, a Sloan Fellowship in Chemistry, and the NIH (2RM1HG006193 and 5U24AI118672). E.R. Edelman was supported, in part, by the NIH (R01GM04903924 and R01 HL161069).

Downloaded from http://ahajournals.org by on July 13, 2026

Downloaded from http://ahajournals.org by on July 13, 2026

Disclosures

A.S. Kalluri reports compensation for consulting from nference, inc. A.K. Shalek reports compensation for consulting and scientific advisory board membership from Merck, Honeycomb Biotechnologies, Cellarity, Repertoire Immune Medicines, Ochre Bio, and Dahlia Biosciences. The other authors report no conflicts.

Supplemental Material

Major Resources Table
Figures S1–S8
Tables S1–S4
Publication and Licensing Rights for the Graphic Abstract, Figures 1A and 2A and Figures S1 and S4A

REFERENCES

1. Pierce RW, Giuliano JS, Pober JS. Endothelial cell function and dysfunction in critically ill children. *Pediatrics*. 2017;140:e20170355. doi: 10.1542/peds.2017-0355
2. García-Cardeña G, Comander J, Anderson KR, Blackman BR, Gimbrone Jr MA. Biomechanical activation of vascular endothelium as a determinant of its functional phenotype. *Proc Natl Acad Sci*. 2001;98:4478–4485. doi: 10.1073/pnas.071052598
3. Krenning G, Barauna VG, Krieger JE, Harmsen MC, Moonen JRAJ. Endothelial plasticity: shifting phenotypes through force feedback. *Stem Cells Int*. 2016;2016:1–15. doi: 10.1155/2016/9762959
4. Tsao CW, Aday AW, Almarzooq ZI, Alonso A, Beaton AZ, Bittencourt MS, Boehme AK, Buxton AE, Carson AP, Commodore-Mensah Y, et al. Heart disease and stroke statistics—2022 update: a report from the American Heart Association. *Circulation*. 2022;145:e153–e639. doi: 10.1161/CIR.0000000000001052
5. Lehoux S, Castier Y, Tedgui A. Molecular mechanisms of the vascular responses to haemodynamic forces. *J Intern Med*. 2006;259:381–392. doi: 10.1111/j.1365-2796.2006.01624.x
6. Chistiakov DA, Orekhov AN, Bobryshev YV. Effects of shear stress on endothelial cells: go with the flow. *Acta Physiol*. 2017;219:382–408. doi: 10.1111/apha.12725
7. Chiu JJ, Chien S. Effects of disturbed flow on vascular endothelium: pathophysiological basis and clinical perspectives. *Physiol Rev*. 2011;91:327–387. doi: 10.1152/physrev.00047.2009
8. Chu TJ, Peters DG. Serial analysis of the vascular endothelial transcriptome under static and shear stress conditions. *Physiol Genomics*. 2008;34:185–192. doi: 10.1152/physiolgenomics.90201.2008
9. Bailey KA, Haj FG, Simon SI, Passerini AG. Atherosusceptible shear stress activates endoplasmic reticulum stress to promote endothelial inflammation. *Sci Rep*. 2017;7:8196. doi: 10.1038/s41598-017-08417-9
10. Scheitlin CG, Julian JA, Shanmughapriya S, Madesh M, Tsoukias NM, Alevriadou BR. Endothelial mitochondria regulate the intracellular Ca2+ response to fluid shear stress. *Am J Physiol Cell Physiol*. 2016;310:C479–C490. doi: 10.1152/ajpcell.00171.2015
11. Xu S, Xu Y, Yin M, Zhang S, Liu P, Koroleva M, Si S, Little PJ, Pelisek J, Jin ZG. Flow-dependent epigenetic regulation of IGFBP5 expression by H3K27me3 contributes to endothelial anti-inflammatory effects. *Theranostics*. 2018;8:3007–3021. doi: 10.7150/thno.21966
12. Levin AD, Vukmirovic N, Hwang CW, Edelman ER. Specific binding to intracellular proteins determines arterial transport properties for rapamycin and paclitaxel. *Proc Natl Acad Sci*. 2004;101:9463–9467. doi: 10.1073/pnas.0400918101
13. Matter CM, Rozenberg I, Jaschko A, Greutert H, Kurz DJ, Wnendt S, Kuttler B, Joch H, Grünenfelder J, Zünd G, et al. Effects of tacrolimus or sirolimus on proliferation of vascular smooth muscle and endothelial cells. *J Cardiovasc Pharmacol*. 2006;48:286–292. doi: 10.1097/01.fjc.0000248233.22570.8b
14. Habib A, Finn AV. Antiproliferative drugs for restenosis prevention. *Interv Cardiol Clin*. 2016;5:321–329. doi: 10.1016/j.iccl.2016.02.002
15. Pasquier E, Honore S, Pourroy B, Jordan MA, Lehmann M, Briand C, Braguer D. Antiangiogenic concentrations of paclitaxel induce an increase in microtubule dynamics in endothelial cells but not in cancer cells. *Cancer Res*. 2005;65:2433–2440. doi: 10.1158/0008-5472.CAN-04-2624
16. Miyakawa AA, Girao-Silva T, Krieger JE, Edelman ER. Rapamycin activates TGF receptor independently of its ligand: implications for endothelial dysfunction. *Clin Sci*. 2018;132:437–447. doi: 10.1042/CS20171457
17. Ma Q, Nie X, Yu M, Wang Z, Yang S, Jia D, Zhou Y. Rapamycin regulates the expression and activity of Krüppel-like transcription factor 2 in human umbilical vein endothelial cells. *PLoS One*. 2012;7:e43315–e43312. doi: 10.1371/journal.pone.0043315
18. Vion AC, Kheloufi M, Hammoutene A, Poisson J, Lasselin J, Devue C, Pic I, Dupont N, Busse J, Stark K, et al. Autophagy is required for endothelial cell alignment and atheroprotection under physiological blood flow. *Proc Natl Acad Sci*. 2017;114:E8675–E8684. doi: 10.1073/pnas.1702223114
19. Rohlenova K, Goveia J, García-Caballero M, Subramanian A, Kalucka J, Treps L, Falkenberg KD, de Rooij LPMH, Zheng Y, Lin L, et al. Single-cell RNA sequencing maps endothelial metabolic plasticity in pathological angiogenesis. *Cell Metab*. 2020;31:862–877.e14. doi: 10.1016/j.cmet.2020.03.009
20. Zhao Q, Eichten A, Parveen A, Adler C, Huang Y, Wang W, Ding Y, Adler A, Nevins T, Ni M, et al. Single-cell transcriptome analyses reveal endothelial cell heterogeneity in tumors and changes following antiangiogenic treatment. *Cancer Res*. 2018;78:2370–2382. doi: 10.1158/0008-5472.CAN-17-2728
21. Kalluri AS, Vellarikkal SK, Edelman ER, Nguyen L, Subramanian A, Ellinor PT, Regev A, Kathiresan S, Gupta RM. Single-cell analysis of the normal mouse aorta reveals functionally distinct endothelial cell populations. *Circulation*. 2019;140:147–163. doi: 10.1161/CIRCULATIONAHA.118.038362
22. He D, Mao A, Zheng CB, Kan H, Zhang K, Zhang Z, Feng L, Ma X. Aortic heterogeneity across segments and under high fat/salt/glucose conditions at the single-cell level. *Natl Sci Rev*. 2020;7:881–896. doi: 10.1093/nsr/nwaa038
23. Andueza A, Kumar S, Kim J, Kang D-W, Mumme HL, Perez JI, Villa-Roel N, Jo H. Endothelial reprogramming by disturbed flow revealed by single-cell RNA and chromatin accessibility study. *Cell Rep*. 2020;33:108491. doi: 10.1016/j.celrep.2020.108491
24. Hughes TK, Wadsworth MH, Gierahn TM, Do T, Weiss D, Andrade PR, Ma F, de Andrade Silva BJ, Shao S, Tsoi LC, et al. Second-strand synthesis-based massively parallel scRNA-seq reveals cellular states and molecular features of human inflammatory skin pathologies. *Immunity*. 2020;53:878–894.e7. doi: 10.1016/j.immuni.2020.09.015
25. Liu Z, Ruter DL, Quigley K, Tanke NT, Jiang Y, Bautch VL. Single-cell RNA sequencing reveals endothelial cell transcriptome heterogeneity under homeostatic laminar flow. *Arterioscler Thromb Vasc Biol*. 2021;41:2575–2584. doi: 10.1161/ATVBAHA.121.316797
26. Rosàs E, Santomá P, Duran-Frigola M, Hernandez B, Llinàs MC, Ruiz-González R, Nonell S, Sánchez-García D, Edelman ER, Balcells M. Modifications of microvascular EC surface modulate phototoxicity of a porphycene anti-ICAM-1 immunoconjugate; therapeutic implications. *Langmuir*. 2013;29:9734–9743. doi: 10.1021/la401067d
27. Wang HJ, Lu TL, Huang H, Huang HC. Paclitaxel induces thrombomodulin downregulation in human aortic endothelial cells. *Tex Heart Inst J*. 2011;38:20–26.
28. Gierahn TM, Wadsworth MH, Hughes TK, Bryson BD, Butler A, Satija R, Fortune S, Love JC, Shalek AK. Seq-well: portable, low-cost RNA sequencing of single cells at high throughput. *Nat Methods*. 2017;14:395–398. doi: 10.1038/nmeth.4179
29. Butler A, Hoffman P, Smibert P, Papalexi E, Satija R. Integrating single-cell transcriptomic data across different conditions, technologies, and species. *Nat Biotechnol*. 2018;36:411–420. doi: 10.1038/nbt.4096
30. Satija R, Farrell JA, Gennert D, Schier AF, Regev A. Spatial reconstruction of single-cell gene expression data. *Nat Biotechnol*. 2015;33:495–502. doi: 10.1038/nbt.3192
31. Love MI, Huber W, Anders S. Moderated estimation of fold change and dispersion for RNA-seq data with DESeq2. *Genome Biol*. 2014;15:1–21. doi: 10.1186/s13059-014-0550-8
32. Cai James J. scGEAToolbox. a Matlab toolbox for single-cell RNA sequencing data analysis. *Bioinformatics*. 2020;36:1948–1949. doi: 10.1093/bioinformatics/btz830
33. Korotkevich G, Sukhov V, Budin N, Shpak B, Artyomov MN, Sergushichev A. Fast gene set enrichment analysis. *BioRxiv*. 2016;2016:60012. doi: 10.1101/060012
34. Liberzon A, Birger C, Thorvaldsdóttir H, Ghandi M, Mesirov JP, Tamayo P. The molecular signatures database hallmark gene set collection. *Cell Syst*. 2015;1:417–425. doi: 10.1016/j.cels.2015.12.004
35. Holland CH, Tanevski J, Perales-Patón J, Gleixner J, Kumar MP, Mereu E, Joughin BA, Stegle O, Lauffenburger DA, Heyn H, et al. Robustness and applicability of transcription factor and pathway analysis tools on single-cell RNA-seq data. *Genome Biol*. 2020;21:1–19. doi: 10.1186/s13059-020-1949-z
36. Alvarez MJ, Shen Y, Giorgi FM, Lachmann A, Ding BB, Ye BH, Califano A. Functional characterization of somatic mutations in cancer using network-based inference of protein activity. *Nat Genet*. 2016;48:838–847. doi: 10.1038/ng.3593
37. Langfelder P, Horvath S. WGCNA. An R package for weighted correlation network analysis. *BMC Bioinf*. 2008;9:1–13. doi: 10.1186/1471-2105-9-559
38. Kazer SW, Aicher TP, Muema DM, Carroll SL, Ordovas-Montanes J, Miao VN, Tu AA, Ziegler CGK, Nyquist SK, Wong EB, et al. Integrated single-cell

analysis of multicellular immune dynamics during hyperacute HIV-1 infection. *Nat Med*. 2020;26:511–518. doi: 10.1038/s41591-020-0799-2
39. Trapnell C, Cacchiarelli D, Grimsby J, Pokharel P, Li S, Morse M, Lennon NJ, Livak KJ, Mikkelsen TS, Rinn JL. The dynamics and regulators of cell fate decisions are revealed by pseudotemporal ordering of single cells. *Nat Biotechnol*. 2014;32:381–386. doi: 10.1038/nbt.2859
40. Deleted in proof.
41. Hazell GGJ, Peachey AMG, Teasdale JE, Sala-Newby GB, Angelini GD, Newby AC, White SJ. PI16 is a shear stress and inflammation-regulated inhibitor of MMP2. *Sci Rep*. 2016;6:39553. doi: 10.1038/srep39553
42. Dolan JM, Sim FJ, Meng H, Kolega J. Endothelial cells express a unique transcriptional profile under very high wall shear stress known to induce expansive arterial remodeling. *Am J Physiol Cell Physiol*. 2012;302:C1109–C1118. doi: 10.1152/ajpcell.00369.2011
43. Daubon T, Léon C, Clarke K, Andrique L, Salabert L, Darbo E, Pineau R, Guérit S, Maitre M, Dedieu S, et al. Deciphering the complex role of thrombospondin-1 in glioblastoma development. *Nat Commun*. 2019;10:1146. doi: 10.1038/s41467-019-08480-y
44. James PD, Goodeve AC. von Willebrand disease. *Genet Med*. 2011;13:365–376. doi: 10.1097/GIM.0b013e3182035931
45. Rocha SF, Schiller M, Jing D, Li H, Butz S, Vestweber D, Biljes D, Drexler HCA, Nieminen-Kelhä M, Vajkoczy P, et al. ESM1 modulates endothelial tip cell behavior and vascular permeability by enhancing VEGF bioavailability. *Circ Res*. 2014;115:581–590. doi: 10.1161/CIRCRESAHA.115.304718
46. Xu Z, Maiti D, Kisiel W, Duh EJ. Tissue factor pathway inhibitor-2 is upregulated by vascular endothelial growth factor and suppresses growth factor-induced proliferation of endothelial cells. *Arterioscler Thromb Vasc Biol*. 2006;26:2819–2825. doi: 10.1161/01.ATV.0000248731.55781.87
47. Liu Y, Chen BPC, Lu M, Zhu Y, Stemerman MB, Chien S, Shyy JYJ. Shear stress activation of SREBP1 in endothelial cells is mediated by integrins. *Arterioscler Thromb Vasc Biol*. 2002;22:76–81. doi: 10.1161/hq0102.101822
48. Lu Q, Longo FM, Zhou H, Massa SM, Chen YH. Signaling through Rho GTPase pathway as viable drug target. *Curr Med Chem*. 2009;16:1355–1365. doi: 10.2174/092986709787846569
49. Choi CK, Helmke BP. Short-term shear stress induces rapid actin dynamics in living endothelial cells. *Mol Cell Biomech*. 2008;5:247–258.
50. Baeyens N, Nicoli S, Coon BG, Ross TD, den Dries K, Han J, Lauridsen HM, Mejean CO, Eichmann A, Thomas JL, et al. Vascular remodeling is governed by a VEGFR3-dependent fluid shear stress set point. *Elife*. 2015;4:e04645. doi: 10.7554/eLife.04645
51. Jiang YZ, Jiménez JM, Ou K, McCormick ME, Zhang LD, Davies PF. Hemodynamic disturbed flow induces differential DNA methylation of endothelial Kruppel-like factor 4 promoter in vitro and in vivo. *Circ Res*. 2014;115:32–43. doi: 10.1161/CIRCRESAHA.115.303883
52. Evellin S, Galvagni F, Zippo A, Neri F, Orlandini M, Incarnato D, Dettori D, Neubauer S, Kessler H, Wagner EF, et al. FOSL1 controls the assembly of endothelial cells into capillary tubes by direct repression of αv and β3 integrin transcription. *Mol Cell Biol*. 2013;33:1198–1209. doi: 10.1128/MCB.01054-12
53. Chai X, Yan J, Gao Y, Jin J. Endothelial HNF4α potentiates angiogenic dysfunction via enhancement of vascular endothelial growth factor resistance in T2DM. *J Cell Biochem*. 2019;120:12989–13000. doi: 10.1002/jcb.28570
54. Ni W, Watts SW, Ng M, Chen S, Glenn DJ, Gardner DG. Elimination of vitamin D receptor in vascular endothelial cells alters vascular function. *Hypertension*. 2014;64:1290–1298. doi: 10.1161/HYPERTENSIONAHA.114.03971
55. Mussbacher M, Salzmann M, Brostjan C, Hoesel B, Schoergenhofer C, Datler H, Hohensinner P, Basílio J, Petzelbauer P, Assinger A, et al. Cell type-specific roles of NF-κB linking inflammation and thrombosis. *Front Immunol*. 2019;10:85. doi: 10.3389/fimmu.2019.00085
56. Yokoyama M, Shimizu I, Nagasawa A, Yoshida Y, Katsuumi G, Wakasugi T, Hayashi Y, Ikegami R, Suda M, Ota Y, et al. p53 plays a crucial role in endothelial dysfunction associated with hyperglycemia and ischemia. *J Mol Cell Cardiol*. 2019;129:105–117. doi: 10.1016/j.yjmcc.2019.02.010
57. Qiao M, Shapiro P, Fosbrink M, Rus H, Kumar R, Passaniti A. Cell cycle-dependent phosphorylation of the RUNX2 transcription factor by cdc2 regulates endothelial cell proliferation. *J Biol Chem*. 2006;281:7118–7128. doi: 10.1074/jbc.M508162200
58. Vuong LM, Chellappa K, Dhahbi JM, Deans JR, Fang B, Bolotin E, Titova NV, Hoverter NP, Spindler SR, Waterman ML, et al. Differential effects of hepatocyte nuclear factor 4α isoforms on tumor growth and T-cell factor 4/AP-1 interactions in human colorectal cancer cells. *Mol Cell Biol*. 2015;35:3471–3490. doi: 10.1128/MCB.00030-15
59. Savory JGA, Bouchard N, Pierre V, Rijli FM, De Repentigny Y, Kothary R, Lohnes D. Cdx2 regulation of posterior development through non-Hox targets. *Development*. 2009;136:4099–4110. doi: 10.1242/dev.041582
60. Cogburn LA, Trakooljul N, Wang X, Ellestad LE, Porter TE. Transcriptome analyses of liver in newly-hatched chicks during the metabolic perturbation of fasting and re-feeding reveals THRSPA as the key lipogenic transcription factor. *BMC Genomics*. 2020;21:1–34. doi: 10.1186/s12864-020-6525-0
61. Bocci G, Di Paolo A, Danesi R. The pharmacological bases of the anti-angiogenic activity of paclitaxel. *Angiogenesis*. 2013;16:481–492. doi: 10.1007/s10456-013-9334-0
62. Weaver BA. How Taxol/paclitaxel kills cancer cells. *Mol Biol Cell*. 2014;25:2677–2681. doi: 10.1091/mbc.E14-04-0916
63. Zamora A, Alves M, Chollet C, Therville N, Fougeray T, Tatin F, Franchet C, Gomez-Brouchet A, Vaysse C, Martinez LO, et al. Paclitaxel induces lymphatic endothelial cells autophagy to promote metastasis. *Cell Death Dis*. 2019;10:956. doi: 10.1038/s41419-019-2181-1
64. Park-Windhol C, Ng YS, Yang J, Primo V, Saint-Geniez M, D'Amore PA. Endomucin inhibits VEGF-induced endothelial cell migration, growth, and morphogenesis by modulating VEGFR2 signaling. *Sci Rep*. 2017;7:17138. doi: 10.1038/s41598-017-16852-x
65. Balatskyi VV, Dobrzyn P. Role of stearoyl-CoA desaturase 1 in cardiovascular physiology. *Int J Mol Sci*. 2023;24:5531. doi: 10.3390/ijms24065531
66. Gasic I, Boswell SA, Mitchison TJ. Tubulin mRNA stability is sensitive to change in microtubule dynamics caused by multiple physiological and toxic cues. *PLoS Biol*. 2019;17:e3000225. doi: 10.1371/journal.pbio.3000225
67. Kim JW, Kim TD, Hong BS, Kim OY, Yoon WH, Chae CB, Gho YS. A serum-stable branched dimeric anti-VEGF peptide blocks tumor growth via anti-angiogenic activity. *Exp Mol Med*. 2010;42:514–523. doi: 10.3858/emm.2010.42.7.052
68. Neill G, Masson GR. A stay of execution: ATF4 regulation and potential outcomes for the integrated stress response. *Front Mol Neurosci*. 2023;16:1112253. doi: 10.3389/fnmol.2023.1112253
69. Michalik KM, You X, Manavski Y, Doddaballapur A, Zörnig M, Braun T, John D, Ponomareva Y, Chen W, Uchida S, et al. Long noncoding RNA MALAT1 regulates endothelial cell function and vessel growth. *Circ Res*. 2014;114:1389–1397. doi: 10.1161/CIRCRESAHA.114.303265
70. Ott EB, Van Den Akker NMS, Sakalis PA, Gittenberger-de Groot AC, Te Velthuis AJW, Bagowski CP. The lim domain only protein 7 is important in zebrafish heart development. *Dev Dyn*. 2008;237:3940–3952. doi: 10.1002/dvdy.21807
71. Lerchenmüller C, Heißenberg J, Damilano F, Bezzeridis VJ, Krämer I, Bochaton-Piallat ML, Hirschberg K, Busch M, Katus HA, Peppel K, et al. S100A6 regulates endothelial cell cycle progression by attenuating antiproliferative signal transducers and activators of transcription 1 signaling. *Arterioscler Thromb Vasc Biol*. 2016;36:1854–1867. doi: 10.1161/ATVBAHA.115.306415
72. Watari K, Shibata T, Fujita H, Shinoda A, Murakami Y, Abe H, Kawahara A, Ito H, Akiba J, Yoshida S, et al. NDRG1 activates VEGF-A-induced angiogenesis through PLCγ1/ERK signaling in mouse vascular endothelial cells. *Commun Biol*. 2020;3:107. doi: 10.1038/s42003-020-0829-0
73. Liang X, Su Y, Huo Y. Forkhead box protein O1 (FoxO1)/SERPINB1 ameliorates ROS production in diabetic nephropathy. *Food Sci Nutr*. 2021;9:44–51. doi: 10.1002/fsn3.1859
74. Zanin R, Pegoraro S, Ros G, Ciani Y, Piazza S, Bossi F, Bulla R, Zennaro C, Tonon F, Lazarevic D, et al. HMGA1 promotes breast cancer angiogenesis supporting the stability, nuclear localization and transcriptional activity of FOXM1. *J Exp Clin Cancer Res*. 2019;38:1–23. doi: 10.1186/s13046-019-1307-8
75. Ma SC, Li Q, Peng JY, Zhouwen JL, Diao JF, Niu JX, Wang X, Guan XD, Jia W, Jiang WG. Claudin-5 regulates blood-brain barrier permeability by modifying brain microvascular endothelial cell proliferation, migration, and adhesion to prevent lung cancer metastasis. *CNS Neurosci Ther*. 2017;23:947–960. doi: 10.1111/cns.12764
76. Young SK, Shao Y, Bidwell JP, Wek RC. Nuclear matrix protein 4 is a novel regulator of ribosome biogenesis and controls the unfolded protein response via repression of Gadd34 expression. *J Biol Chem*. 2016;291:13780–13788. doi: 10.1074/jbc.M116.729830
77. Guan BJ, Krokowski D, Majumder M, Schmotzer CL, Kimball SR, Merrick WC, Koromilas AE, Hatzoglou M. Translational control during endoplasmic reticulum stress beyond phosphorylation of the translation initiation factor eIF2α. *J Biol Chem*. 2014;289:12593–12611. doi: 10.1074/jbc.M113.543215
78. Knupp J, Arvan P, Chang A. Increased mitochondrial respiration promotes survival from endoplasmic reticulum stress. *Cell Death Differ*. 2019;26:487–501. doi: 10.1038/s41418-018-0133-4

Downloaded from http://ahajournals.org by on July 13, 2026